

Evaluation of liquefaction strength of Japanese natural sandy soil using triaxial and simple shear tests

Fusao Oka, Akihiko Oshima, Haruo Fukai

[Outlines]

Natural soil behavior exhibits anisotropy due to particle shape and deposition mode.

→ Suitable experimental method required

Earthquake loading is similar to simple shear test

→ Cyclic torsional simple test is more appropriate.

→ However, due to the practicality, cyclic triaxial test is also well used.

CSR or liquefaction strength are highly variable depending on stress conditions.

Experiments with controlled stress conditions are required.

[Method]

Compare liquefaction strength of natural sand by cyclic triaxial & cyclic simple shear tests.

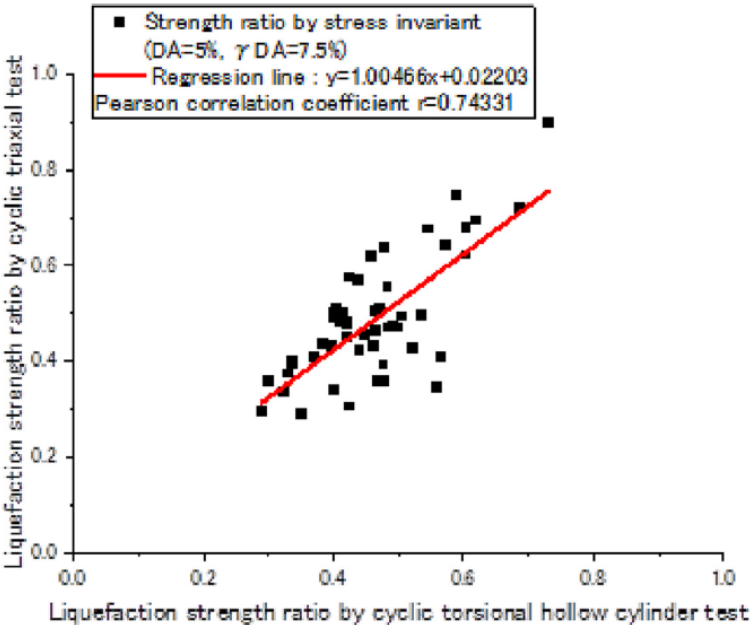
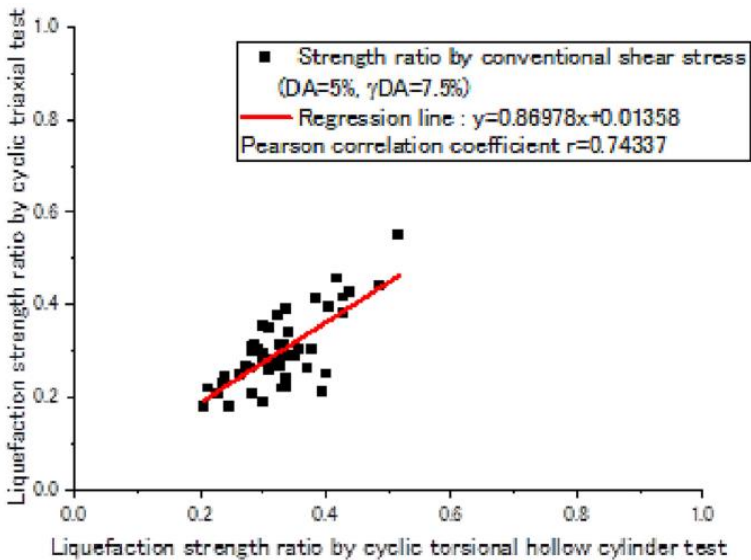
Using stress invariants to determine liquefaction strength.

[Results]

Using conventional stress ratio, liquefaction strength from triaxial tests was generally lower than from torsional hollow cylindrical tests, with regression line slope not being 1.0.

In contrast, stress invariant ratio showed a nearly perfect correlation between the two tests.

However, deviations remained due to interactions between soil fabric and loading mode, suggesting future research should focus on these factors.



Frequency- and intensity-dependent impedance functions of laterally loaded pile groups in cohesionless soil

Naba Raj Shrestha, Masato Saitoh, Chandra Shekhar Goit, Alok Kumer Saha, Ryoya Yokota

[Outlines]

Dynamic loads influence piles response

Soil-structure interaction (SSI) play a significant role.

Soil-pile interaction problem under large-amplitude loading.

Direct approach using BDM is difficult in incorporating soil’s nonlinear behavior.

→ Substructure approaches to analyze the inertial SSI.

Focuses on understanding how frequency and amplitude of loads affect loaded pile group.

[Methods]

2×2 model pile group, experiments with a laminar shear box attached to a shaking table.

Applied load: quasi-static and dynamic lateral loads.

The horizontal impedance functions:

Evaluated by analyzing force-displacement relationships & stereo-PIV techniques

[Results]

At 6~15 Hz, Real part of the impedance functions decreased with increasing loading amplitude.

At higher frequencies, soil-pile system stiffness decreased due to strain-dependent behavior.

The study found that the dynamic stiffness of the pile groups approached the secant static stiffness of the backbone curve as loading amplitude increased, indicating reduced frequency dependency.

BDM: Boundary element modeling

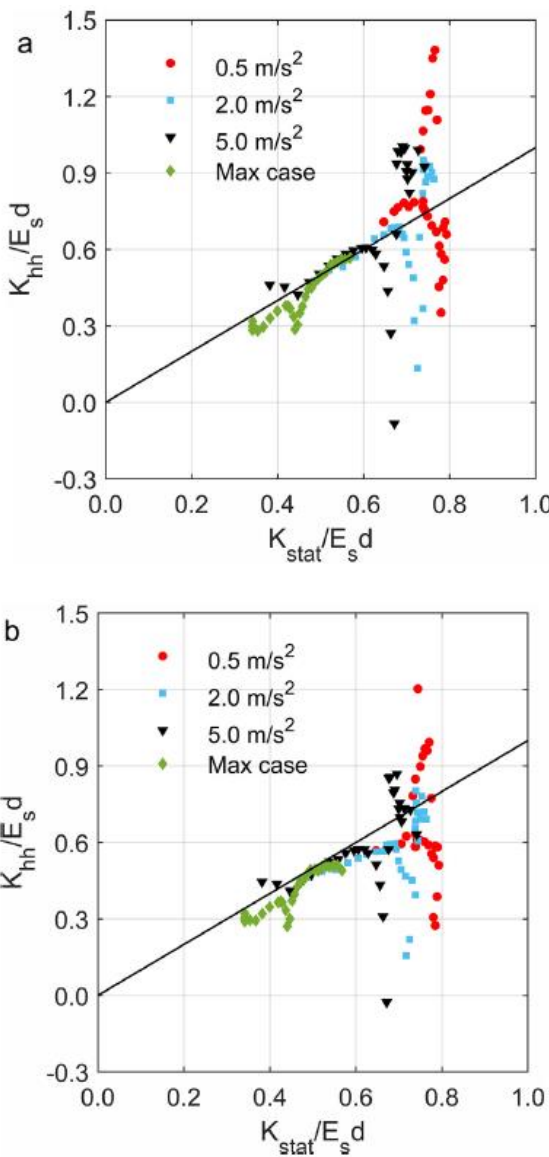


Fig. 12. Comparison between secant stiffness using backbone curve for corresponding displacement amplitude of dynamic Ifs: (a) initial cases and (b) residual cases.

Geotechnical properties of soft clays along Yangon River – Characteristics of soft clays in Thilawa Port area

Yoshimitsu Yamada, Takashi Tsuchida, Nyan Myint Kyaw, Tatsuru Aoyama, Toshiya Akasaki, Moe Myint Su Hlaing, Ryota Hashimoto

[Outline]

Large-scale development projects like the Thilawa Port Development Project.

→ Soft clays sedimented along the Yangon River in Myanmar

Mechanical properties on soft clay sediment is required

Determine the design parameters using samples taken by fixed piston sampler.

[Methods]

Survey + fixed piston sampler & Shelby tube sampler.

Unconfined compression tests and consolidation tests.

[Results]

Fixed piston sampler is better than Shelby tube sampler.

OCR for on-land sites was around 1.4 at shallow depths, indicating overconsolidation due to drying, while the river sites showed OCRs ranging from 1.0 to 6.0, attributed to sedimentation and erosion.

c_v is smaller than that of Japanese marine clay and Vietnam clay, with an average 57.3 cm²/day, fitting well within the log-normal distribution for c_v values less than 225 cm²/day.

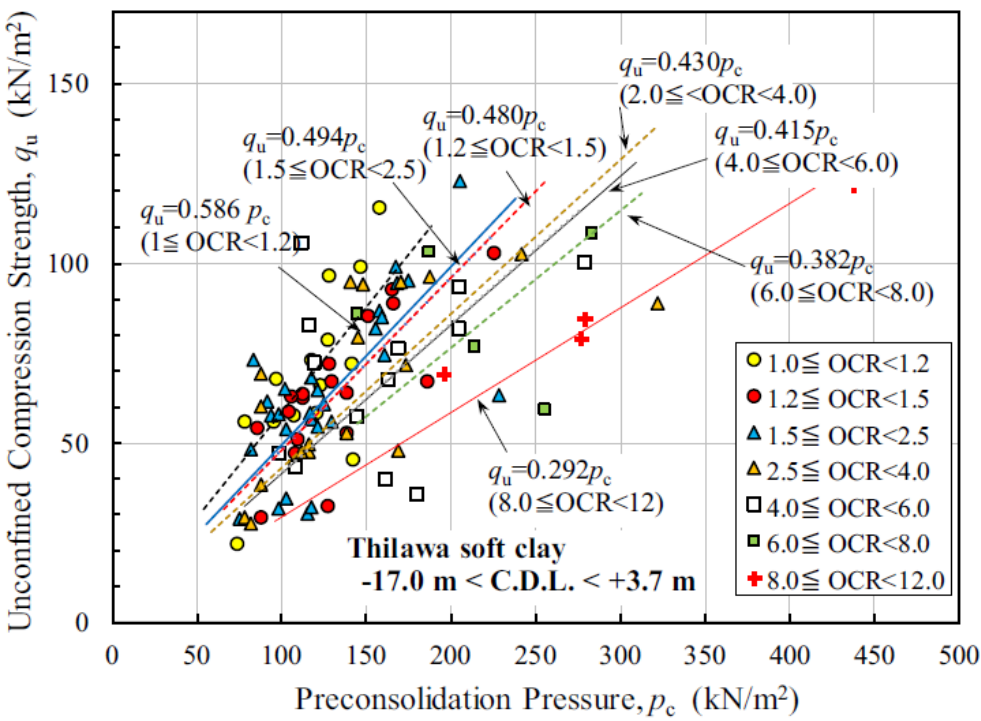


Fig. 16. Relationship between unconfined compressive strength (q_u) and preconsolidation pressure (p_c).

Insights on the role of local site effects on damage distribution in the Izmir metropolitan area induced by the October 30, 2020 Samos earthquake
Anna Chiaradonna, Eyyub Karakan, Cem Kincal, Giuseppe Lanzo, Paola Monaco, Alper Sezer, Mourad Karray

[Outline]

Izmir during the October 30, 2020, Samos earthquake.

→ huge damage even far away from the epicenter

Understand the role of local site effects is required.

→ especially, basin and valley effects

→ local concentrated damage

[Methods]

survey of the damage distribution across 30 districts in Izmir

Seismic data recorded analyze ↔ ground motion characteristics

Ground-motion prediction equations (GMPEs)

→ assess intensity of recorded motions and damage patterns.

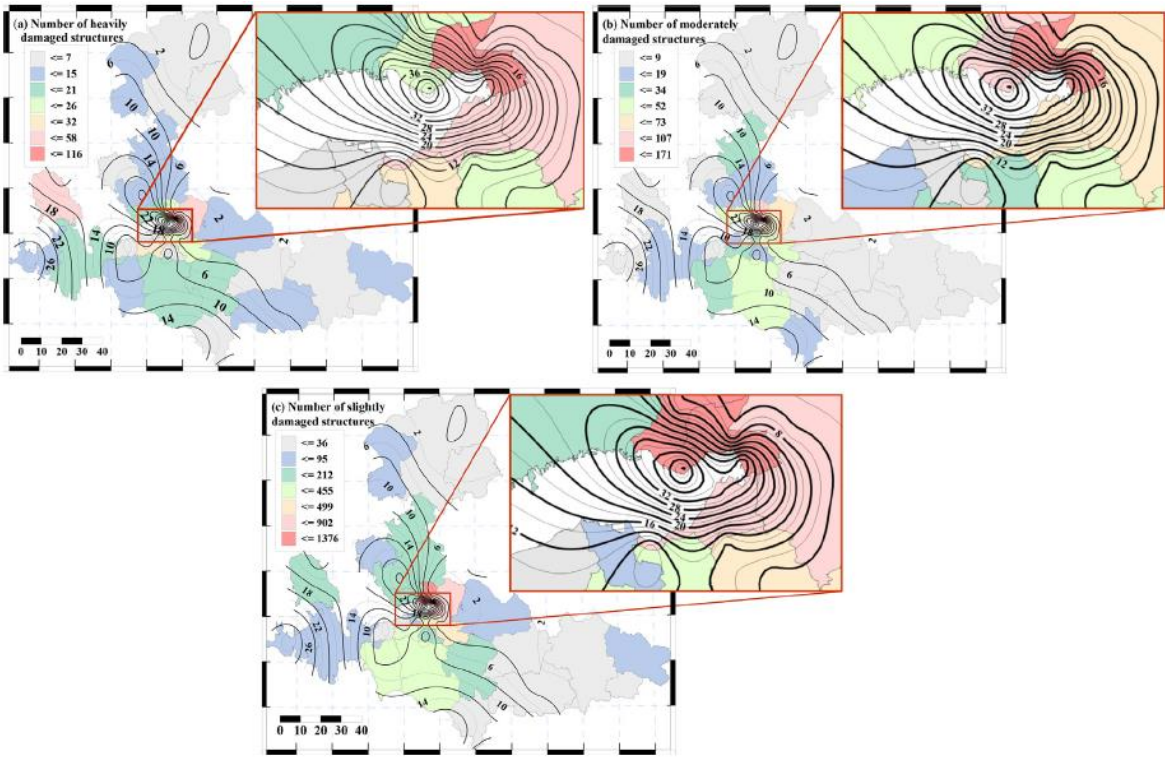


Fig. 8. The number of a) heavily, b) moderately and c) slightly damaged structures in inhabited areas of Izmir metropolitan municipality correlated with contours of Arias intensity (in cm/s).

[Results]

PGA recorded in Izmir's alluvial regions reached up to 0.15 g, significantly higher than values predicted by GMPEs.

Amplification factors between different soil classes and rock sites ranged from 2.2 for PGA to 4 for spectral accelerations at periods of 1 and 3 seconds.

Damage was heavily concentrated in Bornova and Karsiyaka districts, with a clear correlation to double resonance effects and the presence of soft sediments, leading to severe structural damage.

In-situ horizontal cyclic loading tests on composite foundation composed of soilbags and piles

Tatsuya Doi, Yoshitaka Murono, Feng Zhang, Yuji Hirayama

[Outline]

Bending moments in pile heads of composite foundations during earthquakes.
Soil bags countermeasure between pile heads and footings.

Methods

In-situ horizontal cyclic loading tests

{horizontal cyclic loads at varying amplitudes}

→ {observe foundation response under seismic conditions}.

Measurements: horizontal and vertical loads, displacements, inclinations, earth pressures, and strains to analyze the load distribution, deformation, and damping characteristics.

Results

Composite foundation achieved larger hysteresis damping (over 20%) compared to conventional spread foundations, with peak horizontal loads reaching up to 150 kN due to footing uplift.

Axial force in piles was distributed unevenly, with front pile bearing up to 91 kN, while bending moments peaked at around 1.0 m from pile heads.

Despite cyclic loading, the soil bags showed minimal damage, confirming the effectiveness of the composite foundation in reducing bending moments and maintaining structural integrity under seismic loads.

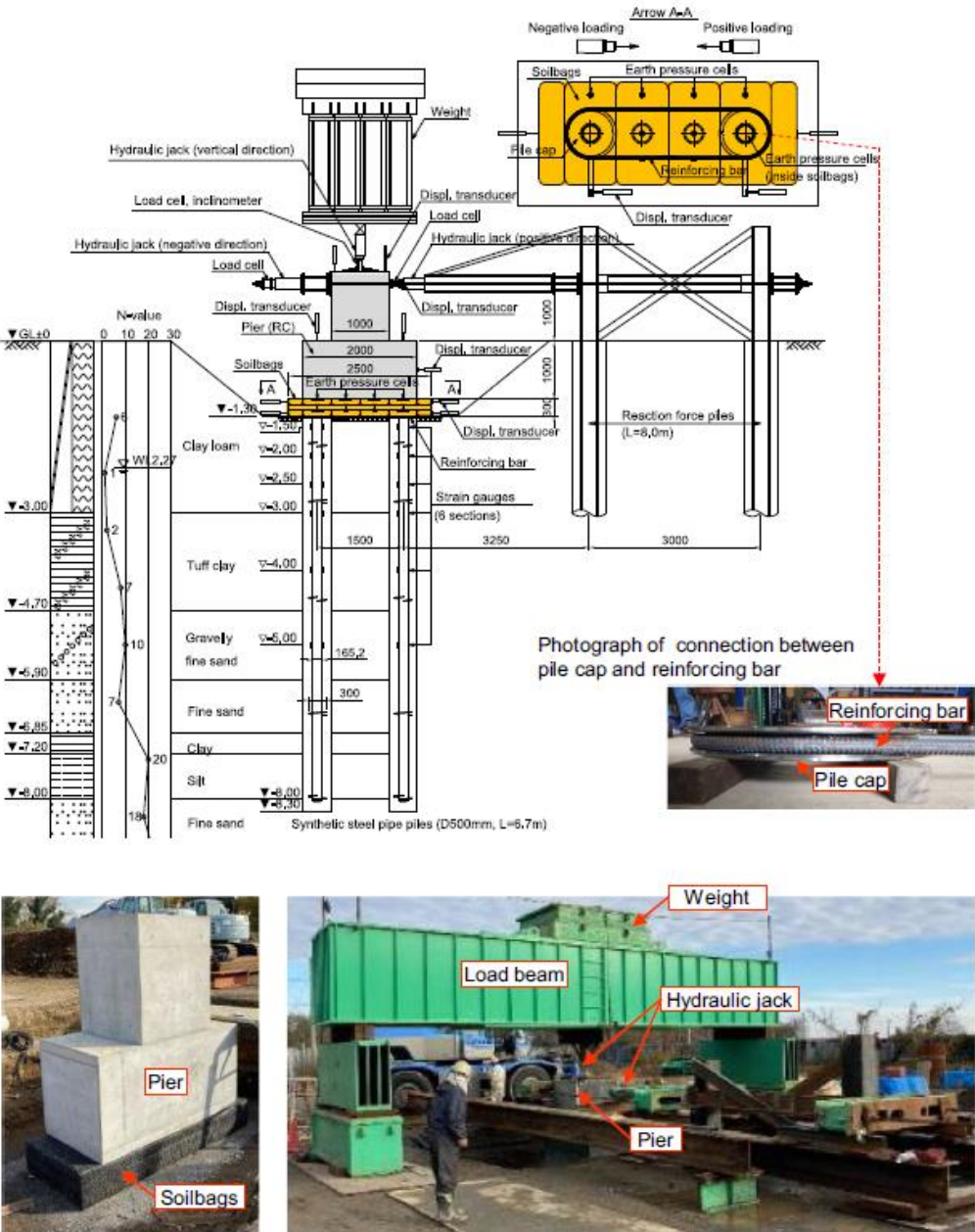


Fig. 4. Overview of in-situ horizontal cyclic loading tests on 2-pile PCF.

Conclusion memo

PCF의 수평 하중과 변위 관계:	변위 증가에 따라 기초의 들림 현상으로 수평 하중이 최대값에 도달. 이로 인해 대형 지진 시 교각 및 말뚝의 관성 반응이 감소. 작은 변위에서는 방추형 이력곡선, 큰 변위에서는 역 S자형 이력곡선을 보임.
뒤 채움 흙 없이 시행된 실험:	이전 연구에서 뒤 채움 흙이 없는 확산 기초와 비교해 기원 지향 성향이 덜 뚜렷. 이는 흙주머니의 전단 변형 이력 효과 때문.
교각의 변형 경향:	반복 하중 시 교각 상단의 들림 및 기초의 침하로 인한 하향 변형 발생. 전반적인 변형은 하향 침하가 주류.
흙주머니의 수직 토압 분포:	말뚝 머리 위에서 큰 토압, 말뚝 사이 기초 지반 위에서 작은 토압. 이는 말뚝 머리의 강성이 기초 지반보다 훨씬 크기 때문. 수평 반복 하중 시 흙주머니의 수직 토압은 하중 방향 전면에 집중.
말뚝 머리의 굽힘 모멘트:	수평 하중 시 말뚝 머리 근처의 굽힘 모멘트는 작음. 말뚝 머리에서 약 1.0m 아래에서 굽힘 모멘트가 최대. 이는 흙주머니로 인해 말뚝과 기초가 절연되고, 말뚝 머리의 회전 제약 조건이 자유 조건에 가까워서 발생.
말뚝의 축력과 굽힘 모멘트:	전면 말뚝의 축력과 굽힘 모멘트가 후면 말뚝보다 큼. 수평 하중이 양쪽 말뚝 머리를 연결하는 철근에 의해 균등하게 나뉘지지 않음. ±60mm 하중 이후 철근의 축력이 크게 증가, 대형 지진 시 철근이 수평 하중을 균등하게 분담함을 의미.
현장 실험 결과와 이전 연구 결과 일치:	이번 현장 실험 결과는 이전의 모델 흔들림 테이블 실험 및 수치 실험 결과와 일치. 이는 실제 응력 수준에서 PCF의 효과가 입증됨.
흙주머니의 내구성:	실제 규모의 수평 반복 하중 실험 중 흙주머니는 손상되지 않음. 일부 흙주머니의 지오텍스타일이 부분적으로 마모된 한 곳을 제외하고 흙주머니는 충분한 압축 강도를 가짐. 이는 대형 지진 시 철도 교각 기초 아래의 흙주머니가 충분한 압축 강도를 가진다는 것을 의미.

Novel method for evaluating water absorption and retention of waste-based stabilizers using suction filtration to predict treatment effects on soft clay soils Alula Kassa, Shovon Raihan, Kimitoshi Hayano, Binh Nguyen Phan, Hiromoto Yamauchi, Yoshitoshi Mochizuki

[Outline] Cement soil stabilization is energy-intensive and carbon dioxide emissions.
New method of water absorption and retention capacities of waste-based stabilizers.
By using suction filtration, this method seeks to improve the efficiency and accuracy of predicting the treatment effects of stabilizers on soft clay soils.

[Methods] Suction filtration method to measure the water absorption and retention of various waste-based stabilizers, fly ash (FA), paper sludge ash-based stabilizer (PSAS), biomass ash (BMA), and their hybrids.
Cone index tests → performance of stabilizers was evaluated.

[Results] PSAS stabilizer is best for water absorption and retention rate → $PSAS \geq PSAS\text{-}BMA \text{ hybrid} > BMA > FA$
Peak cone index (q_c) → $PSAS (q_c=300 \text{ kPa}) > FA (q_c=200 \text{ kPa})$ and $BMA (q_c=250 \text{ kPa})$
Modified water content (w^*), which considers absorbed water as a solid, correlated better with q_c .

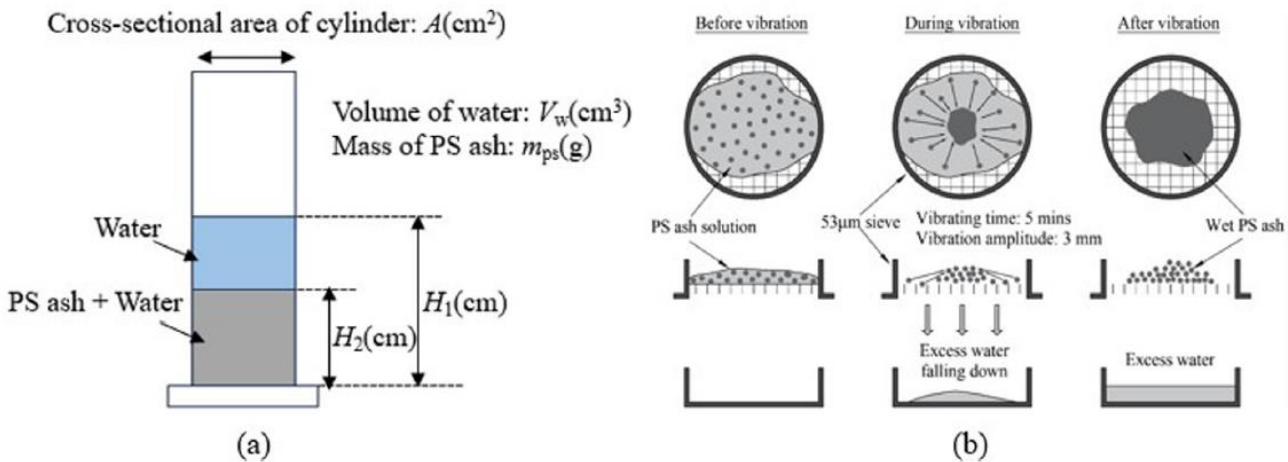


Fig. 2. Schematic of method for evaluation of water absorption and retention of PSASs: (a) cylinder method (Kato et al., 2005) and (b) sieve method (Phan et al., 2021).

Numerical investigation into composite behavior of over-deformed segmental tunnel linings strengthened by bonding steel plates
Wuzhou Zhai, Dongming Zhang, Hongwei Huang, David Chapman

[Outline]

Problem of excessive deformation in segmental tunnel linings.
→ Investigate effectiveness of strengthening linings by bonding steel plates
{mainly to enhance stiffness}, {load-bearing capacity of tunnels}

[Methods]

FEM-ABAQUS; simulate segmental tunnel linings strengthened with steel plates.
Cohesive zone modeling; the interface bonding behavior between the tunnel lining and the steel plates.

[Results]

Strengthened tunnel linings exhibited significant improvements in stiffness and load-bearing capacity.
Interface shear stress concentration occurred at segment joints.
Maximum tensile stress in steel plates reached 49.9 MPa near tunnel crown, while compressive stress peaked at 23.3 MPa near tunnel spring line.
Delaying the strengthening increased tunnel's load-bearing capacity by 35.2% but decreased its stiffness by 45.5%.

Except tunnel, Is this geotechnical research?

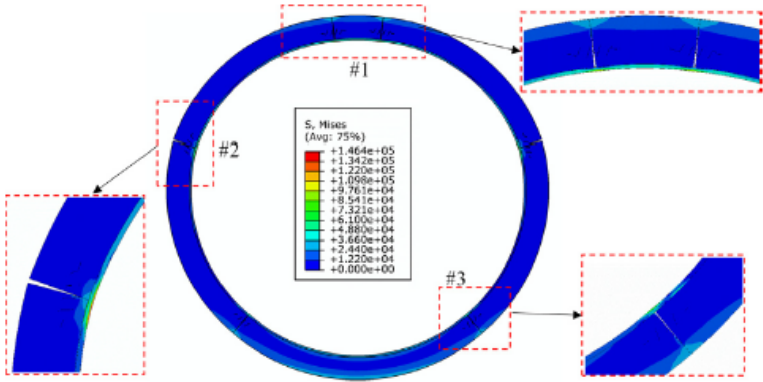


Fig. 12. Stress contour of the segmental tunnel lining strengthened by steel plates.

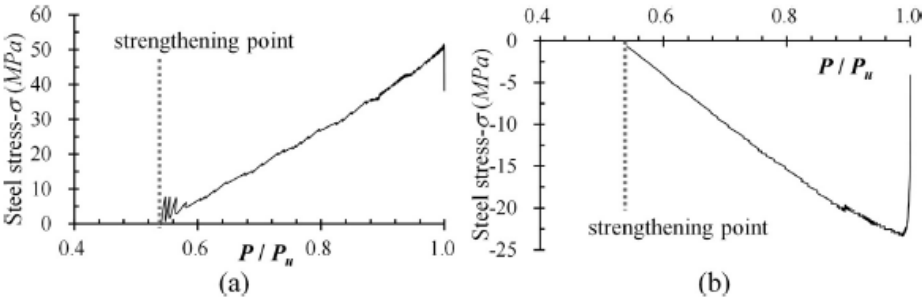


Fig. 13. Stress in the steel plate at different tunnel positions, (a) joint #1, (b) joint #2.